RESEARCH ARTICLE | JANUARY 07 2026

Using stereodynamical portraits to visualize polarized rotational angular momentum distributions in H_2–surface collisions

Helen Chadwick

J. Chem. Phys. 164, 014706 (2026)
https://doi.org/10.1063/5.0312643

The Journal of Chemical Physics ARTICLE pubs.aip.org/aip/jcp

Using stereodynamical portraits to visualize polarized rotational angular momentum distributions in H_2–surface collisions

Cite as: J. Chem. Phys. 164, 014706 (2026); doi: 10.1063/5.0312643
Submitted: 18 November 2025 • Accepted: 11 December 2025 •
Published Online: 7 January 2026

Helen Chadwick[a)]

AFFILIATIONS

Department of Chemistry, Faculty of Science and Engineering, Swansea University, Swansea SA2 8PP, United Kingdom

[a)]Author to whom correspondence should be addressed: h.j.chadwick@swansea.ac.uk

ABSTRACT

The magnetic molecular interferometer (MMI) is a molecular beam scattering apparatus, which allows the polarization of the rotational angular momentum ($\boldsymbol{J}$) of ortho-H_2 molecules to be controlled using tunable magnetic fields before they collide with a surface, and their $\boldsymbol{J}'$ polarization to be determined after the collision. In the current work, quantum population distribution functions, or "stereodynamical portraits," are used to visualize the rotational angular momentum polarization of ortho-H_2 molecules that the MMI creates before the collision with the surface, revealing that the sensitivity of the MMI to stereodynamic effects which depend on the orientation of $\boldsymbol{J}$ with respect to the surface normal can be increased by manipulating the H_2 molecules with two perpendicular magnetic fields rather than just a single field. They can also be used to depict the polarization dependence of a H_2-surface collision, as shown by the example considered here, where it is found that when H_2 molecules undergo diffractive scattering from a Cu(511) surface, different $\boldsymbol{J}$ polarizations are selected to scatter into different diffraction channels, just as different polarizations of $\boldsymbol{J}'$ are created after scattering. Signals measured with the MMI are necessarily dependent on both the rotational polarization the MMI creates and the dependence of the molecule-surface collision on this, and it is demonstrated that for flux detection measurements it would be possible to analyze the data directly in terms of the polarization moments which characterize these two properties to gain a more immediate insight into the stereodynamics of the collision than is possible using alternative analysis methods.

I. INTRODUCTION

Collisions between chemical species are inherently anisotropic, with the outcome not only depending on how energy is partitioned between different molecular degrees of freedom, but also the relative orientation of the species, and the direction from which they approach each other.[1] This dependence on orientation, often referred to as stereodynamics, has been extensively explored in gas-phase collisions,[1–15] for example the role of the initial orientation of the bond axis in the inelastic scattering of NO with rare gas atoms,[6,7] and the effect of collisions both in creating[5,8] and destroying[3,4] initially polarized rotational angular momentum distributions. The idea of vector correlations has been frequently invoked to both quantify the results of the experiments and to provide visualizations that help uncover the underlying mechanisms at a fundamental, molecular level.

Analogous experiments have been performed for molecules colliding with surfaces, for example the effect of orientation of the NO bond axis has also been explored in molecule-surface collisions,[16] as has the effect of initial rotational polarization on determining the probability the molecule dissociates[17–20] and the rotational polarization that can be created by molecules colliding with surfaces.[21–28] While these are also clear demonstrations of stereodynamics, the underpinning idea of describing these in terms of vector correlations is less developed than in gas phase scattering, despite clear parallels between the two. A review by Auerbach, Tully, and Wodtke has highlighted the value of transferring techniques that were originally developed for gas phase scattering

to molecule–surface collisions,[29] and the work presented here will continue that trend.

A collision between a closed shell diatomic molecule and rare gas atom can be fully characterized using the four vector $\boldsymbol{k}$–$\boldsymbol{k}'$–$\boldsymbol{J}$ – $\boldsymbol{J}'$ correlation, which corresponds to the initial ($\boldsymbol{k}$) and final ($\boldsymbol{k}'$) relative velocities and the direction of the rotational angular momentum of the diatom before ($\boldsymbol{J}$) and after ($\boldsymbol{J}'$) the collision.[9,30–32] These four vectors can also be used to describe the collision of a diatomic molecule with a surface, allowing methods that were originally developed to describe gas phase scattering to also be used to describe molecule-surface scattering. The $\boldsymbol{k}$–$\boldsymbol{k}'$–$\boldsymbol{J}$ – $\boldsymbol{J}'$ correlation can be obtained for a single ($\boldsymbol{k}$–$\boldsymbol{k}'$) scattering angle using the magnetic molecular interferometer (MMI), which allows the rotational orientation of hydrogen to be controlled and manipulated both before and after a collision with a surface.[33] Signals measured using the MMI necessarily depend on both the polarization dependence, or stereodynamics, of the scattering process and the rotational polarization of the molecular beam that the MMI creates that collides with the surface. The first of these properties is the intrinsic polarization and depends on the molecule-surface collision only and can be considered to be what the collision wants, whereas the former is the extrinsic polarization characterizing the rotational polarization of the molecules before the collision and so can be changed and can be considered to be what the collision gets.[34–37] Ultimately the goal is to learn as much about the intrinsic polarization dependence of the molecule-surface collision as possible, although the information that can be obtained in a measurement can be limited if the extrinsic polarization is not sensitive to the property, or polarization, of interest.

Previous work using the MMI has shown that the rotational orientation of the molecule affects both the outcome of rotationally elastic scattering of H_2[26,27,33,38] and rotationally inelastic scattering of D_2,[39] as well as controlling the probability of H_2 dissociation.[19] The stereodynamic effects in this work have been analyzed in terms of "helicoptering" and "cartwheeling" molecules with respect to the surface normal, that is, the dependence of the collision with respect to the plane of rotation with respect to a single axis, which corresponds to the rotational alignment. It was shown that the probability of H_2 scattering from a Ni(111) surface could be reproduced by only considering the rotational alignment of the molecules with respect to the surface normal before they collided with the surface.[19] However, only considering this alignment was unable to correctly describe the probability of D_2 undergoing rotationally inelastic scattering from a Cu(111) surface,[39] suggesting that the rotational polarization within the plane of the surface also plays a role, an effect that has been observed previously in O_2 dissociation on surfaces.[40–43]

In the current work, the rotational orientation that the MMI creates in three dimensions will be explored using quantum population distribution functions (QPDFs), or "stereodynamical portraits," an idea originally developed and widely used to visualize vector correlations in gas phase scattering.[12,34,35,37,44–46] It should be noted that these are not the same as classical probability density functions due to the uncertainty in specifying the direction of $\boldsymbol{J}$ quantum mechanically, although the two become the same in the correspondence principle limit.[44,45] The same methodology will be used alongside results from previous work[38] to visualize the intrinsic polarization properties for ortho-H_2 in $J = 1$ scattering elastically from Cu(511) showing the rotational polarization that scatters in to, and from, different diffraction channels. The remainder of the paper is organized as follows. Section II introduces the equations which describe QPDFs[12,35,44,45] as well as the specific details of how these can be calculated in the case of the MMI for both the intrinsic and extrinsic polarizations. The distribution functions for the polarization of $\boldsymbol{J}$ that the MMI creates before scattering are presented in the first part of Sec. III, followed by the polarization of $\boldsymbol{J}$ scattering selects and $\boldsymbol{J}'$ scattering creates in collisions of H_2 with Cu(511). In the final part of Sec. III, these results are combined to demonstrate an alternative method for analyzing MMI measurements which are sensitive to the $\boldsymbol{k}$–$\boldsymbol{k}'$–$\boldsymbol{J}$ correlation, before the final section presents a summary of the work.

II. THEORETICAL METHODS

A. Describing polarized rotational angular momentum (J) distributions

While this section closely follows the theoretical methods developed previously for describing polarized rotational angular momentum distributions in the gas phase,[12,34,35,37,44,45] a different reference frame will be used, which is shown schematically in Fig. 1. In the current work, the XZ plane will be defined as the scattering plane as in gas phase studies, but the direction of the Z-axis will be taken as the surface normal, as opposed to the direction of the initial velocity vector $\boldsymbol{k}$. This choice of reference frame is more logical for gas-surface collisions, as it means that the surface plane corresponds to the XY plane, as well as being consistent with that typically used in theoretical gas-surface studies where the surface normal is taken to be the Z-axis.[47]

The expansion of the QPDF can be written as[12,34,35,37,44,45]

$$P(\theta_J, \phi_J) = \sum_{k=0}^{2J} \sum_{q=-k}^{k} \frac{2k+1}{4\pi} \langle JJ, k0|JJ\rangle a_q^{(k)} C_q^{(k)}(\theta_J, \phi_J)^*, \quad (1)$$

where θ_J and ϕ_J are the polar and azimuthal angles describing the direction of the vector $\boldsymbol{J}$ as shown in Fig. 1, $\langle JJ, k0|JJ\rangle$ is a

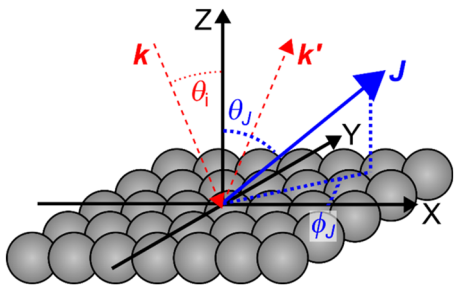

FIG. 1. The reference frame used in the current work for calculating the quantum population distribution functions, showing the initial ($\boldsymbol{k}$) and final ($\boldsymbol{k}'$) velocities and the direction of the rotational angular momentum ($\boldsymbol{J}$). The direction of $\boldsymbol{J}$ is defined by the polar and azimuthal angles θ_J and ϕ_J, and the incident angle of the H_2 is θ_i. The surface normal is along the +Z-axis, the surface lies in the XY plane, and $\boldsymbol{k}$ and $\boldsymbol{k}'$ lie in the XZ plane.

Clebsch–Gordan coefficient which accounts for how accurately the direction of $\boldsymbol{J}$ can be described quantum mechanically, $a_q^{(k)}$ are the (complex) expansion coefficients, $C_q^{(k)}(\theta_J, \phi_J)$ are the modified spherical harmonics,[12,48] and k and q correspond to the order and degree of the polarization that they are describing. This expression can be rewritten in terms of real polarization moments $a_{q\pm}^{\{k\}}$ (note the different brackets which are used to distinguish between the real and complex moments, and that for the real moments $q \geq 0$) as[12,34,35,37,44,45]

$$P(\theta_J, \phi_J) = \sum_{k=0}^{2J} \frac{2k+1}{4\pi} \langle JJ, k0|JJ\rangle \left[a_0^{\{k\}} C_0^{\{k\}}(\theta_J, \phi_J) + \sum_{q=1}^{k} a_{q+}^{\{k\}} C_{q+}^{\{k\}}(\theta_J, \phi_J) + a_{q-}^{\{k\}} C_{q-}^{\{k\}}(\theta_J, \phi_J) \right], \quad (2)$$

where the real $a_{q\pm}^{\{k\}}$ can be found from the complex moments,[12,48]

$$\begin{aligned} a_0^{\{k\}} &= a_0^{(k)}, \\ a_{q+}^{\{k\}} &= \frac{1}{\sqrt{2}}\left[(-1)^q a_{+q}^{(k)} + a_{-q}^{(k)}\right], \quad q > 0, \\ a_{q-}^{\{k\}} &= \frac{1}{i\sqrt{2}}\left[(-1)^q a_{+q}^{(k)} - a_{-q}^{(k)}\right], \quad q > 0, \end{aligned} \quad (3)$$

and it should be noted that analogous expressions hold for $C_{q\pm}^{\{k\}}(\theta_J, \phi_J)$. As the current work focuses on the elastic scattering of H_2 in the $J = 1$ state, the maximum value of k that contributes to the sum is $k = 2$. In this case, the $k = 1$ $a_{q\pm}^{\{k\}}$ moments quantify the orientation of the rotational polarization, which corresponds to the preferred handedness of rotation (i.e., rotating either clockwise or anticlockwise), and the $k = 2$ moments the alignment, which corresponds to preferred planes of rotation (i.e., rotating like a helicopter or a cartwheel). When $q = 0$ the moments quantify the orientation and alignment with respect to the surface normal (Z-axis), whereas when $q \neq 0$ they also contain information about the polarization in the surface (XY) plane. The physical meaning of each of the moments is given in Table I of Ref. 49 alongside explicit expressions for the values of $a_{q\pm}^{\{k\}}$ for $k \leq 2$.

The $a_{q\pm}^{\{k\}}$ moments are calculated using[12,44,45]

$$\frac{a_{q\pm}^{\{k\}}}{a_0^{\{0\}}} = \left\langle T_{q\pm}^{\{k\}} \right\rangle = \frac{Tr\left(\rho T_{q\pm}^{\{k\}}\right)}{Tr(\rho)}, \quad (4)$$

where ρ is a density matrix which can be obtained using either the scattering matrix determined from an MMI experiment or the wavefunction which characterizes the molecules before they collide with the surface (see Secs. II B and II C, respectively), and Tr corresponds to taking the trace of the matrix. The $T_{q\pm}^{\{k\}}$ are the multipolar tensor operators which are found using the linear combinations of Clebsch–Gordan coefficients as follows:[12]

$$\begin{aligned} \left\langle Jm_J \middle| T_0^{\{k\}} \middle| Jm_J' \right\rangle &= \langle Jm_J', k0|Jm_J\rangle, \\ \left\langle Jm_J \middle| T_{q+}^{\{k\}} \middle| Jm_J' \right\rangle &= \frac{1}{\sqrt{2}}\left[(-1)^q \langle Jm_J', kq|Jm_J\rangle + \langle Jm_J', k-q|Jm_J\rangle\right], \quad q > 0, \\ \left\langle Jm_J \middle| T_{q-}^{\{k\}} \middle| Jm_J' \right\rangle &= \frac{1}{i\sqrt{2}}\left[(-1)^q \langle Jm_J', kq|Jm_J\rangle - \langle Jm_J', k-q|Jm_J\rangle\right], \quad q > 0. \end{aligned} \quad (5)$$

It should be noted that the Clebsch–Gordan coefficients $\langle J_1 m_1, J_2 m_2 | J_3 m_3 \rangle$ are real and quantify the probability amplitude that two angular momentum vectors $|J_1 m_1\rangle$ and $|J_2 m_2\rangle$ couple to give a final angular momentum vector $|J_1 J_2 J_3 m_3\rangle$.[12]

B. Obtaining the intrinsic polarization moments from scattering matrices

The change in the wavefunction when a molecule scatters from a surface is characterized by a scattering matrix (S-matrix). In the case of ortho-H_2 in $J = 1$ scattering from a surface, a 3×3 matrix can be used as the m_I (nuclear spin projection) state will be a spectator to the collision. Each complex element within the matrix ($s_{fn}e^{ik_{fn}}$) characterizes how the amplitude and phase of the wavefunction change for each initial m_J state (n) to final m_J' state (f) transition. It therefore embodies all the information about the $\boldsymbol{k}$–$\boldsymbol{k}'$–$\boldsymbol{J}$ – $\boldsymbol{J}'$ correlation. The achiral nature of the scattering places constraints on the scattering matrix elements,[39] which leads to the explicit expression of the scattering matrix for the elastic scattering of H_2 in $J = 1$ below:

$$S = \begin{pmatrix} s_{11}e^{ik_{11}} & s_{10}e^{ik_{10}} & s_{1-1}e^{ik_{1-1}} \\ s_{01}e^{ik_{01}} & s_{00}e^{ik_{00}} & s_{01}e^{i(\pi+k_{01})} \\ s_{1-1}e^{ik_{1-1}} & s_{10}e^{i(\pi+k_{10})} & s_{11}e^{ik_{11}} \end{pmatrix}. \quad (6)$$

As has been shown previously,[26,27,38,50] it is possible to extract the S-matrix by fitting interference signals obtained from MMI measurements for H_2 colliding with various surfaces, and this methodology will not be reproduced here.

To obtain the $\boldsymbol{k}$–$\boldsymbol{k}'$–$\boldsymbol{J}$ – $\boldsymbol{J}'$ correlation, the polarization of $\boldsymbol{J}'$ has to be determined for a given polarization of $\boldsymbol{J}$. While in principle any polarization of $\boldsymbol{J}$ could be chosen, the approach will be described for a molecule in a pure $m_J = 1$ state, that is, $|\psi\rangle = \begin{pmatrix} 1 \\ 0 \\ 0 \end{pmatrix}$. The wavefunction after scattering ($|\psi'\rangle$) is given by $S|\psi\rangle$. Using $|\psi'\rangle$ in Eq. (4) then allows the $a_{q\pm}^{\{k\}}(m_J = 1)$ moments to be obtained, which if used in Eq. (2) then gives the QPDF which allows the polarization of $\boldsymbol{J}'$ to be visualized which corresponds to the initial, polarized, $m_J = 1$ state. The same approach is used for the $m_J = 0$ and $m_J = -1$ states, just changing $|\psi\rangle$ to the corresponding pure state. The values of $a_{q\pm}^{\{k\}}$ for an initially unpolarized beam can be obtained as the weighted average of the three $a_{q\pm}^{\{k\}}(m_J)$ moments, where each weight corresponds to 1/3 (which ensures $a_0^{\{0\}} = 1$), which allows the QPDF for the $\boldsymbol{k}$–$\boldsymbol{k}'$–$\boldsymbol{J}'$ correlation to be visualized.

Analogously, polarization moments which characterize the QDPF of the molecules that scatter into a given channel can also be found for each m_J' state. To ensure appropriate normalization of the $a_{q\pm}^{\{k\}}(m_J')$ moments ($a_0^{\{0\}}(m_J') = 1$) it is necessary to divide by $\mathrm{Tr}(\rho(m_J'))$, as shown in Eq. (4). While these moments can be combined as above to allow the $\boldsymbol{k}$–$\boldsymbol{k}'$–$\boldsymbol{J}$ correlation to be visualized, the weights for each state are not equal as they will not all scatter with equal probability into the final channel. It follows that the values of the $a_{q\pm}^{\{k\}}$ moments which correspond to the $\boldsymbol{k}$–$\boldsymbol{k}'$–$\boldsymbol{J}$ correlation are found as

$$a_{q\pm}^{\{k\}} = \frac{\sum_{m_J'=-1}^{1} Tr(\rho(m_J'))a_{q\pm}^{\{k\}}(m_J')}{\sum_{m_J'=-1}^{1} Tr(\rho(m_J'))}. \quad (7)$$

C. Obtaining the extrinsic polarization moments from the wavefunction of the molecules that collide with the surface

The methods used to calculate the wavefunction of the ortho-H_2 molecules that collide with the surface have been described previously,[26,27,33,38,50,51] but the necessary details will be presented here to provide context for the later results. In brief, it is necessary to propagate the molecules through the magnetic elements that make up the first arm of the beam line.[33] This consists of a magnetic hexapole,[52] a solenoid, and a Helmholtz coil.[53] The probability that each of the 9 initial m_I, m_J states of ortho-H_2 ($I = 1$, $J = 1$) are transmitted through the hexapole is calculated using quasi-classical trajectory calculations.[54] These are denoted $P_{hex}(m_I'', m_J'')$, where the double prime indicates it is the m_I, m_J state at the end of the hexapole with respect to an axis that lies perpendicular to $\boldsymbol{k}$ in the XZ plane (see Fig. S1). The coherent evolution of each of these states through the rest of the beamline is achieved by propagating the states through the magnetic field profile of the machine,[30,53,55] which consists of a solenoid and a Helmholtz coil that generate mutually perpendicular fields, which lie along the direction of $\boldsymbol{k}$ and the Y-axis, respectively, using the Ramsey Hamiltonian.[56] In an MMI experiment, the current in the solenoid is systematically scanned, which changes the magnetic field the molecules experience as they travel through the first arm of the apparatus, which in turn changes the rotational orientation of the molecules that collide with the surface, as will be demonstrated below.

Determining the polarization moments from the wavefunction is more complicated than from the S-matrix, as there are 9 initial m_I'', m_J'' states in the molecular beam, each of which become a coherent superposition of 9 m_I, m_J states at the surface. The calculation of the polarization moment (which quantifies the polarization of the m_J states) is therefore done three times due to the three m_I states for each initial m_I'', m_J'' state. This then has to be repeated for the different velocities that are present in the molecular beam, which are assumed to have a Gaussian distribution (P_v). The final $a_{q\pm}^{\{k\}}(B)$ moment for a given magnetic field (B) therefore needs averaging over the velocity distribution, the initial m_I'', m_J'' state populations (i.e., the probability each of the states is transmitted through the hexapole), and the weight that each of the m_I states in the wavefunction has at the surface. This is given by

$$a_{q\pm}^{\{k\}}(B) = \frac{\sum_v P_v \sum_{m_I'', m_J''} P_{hex}(m_I'', m_J'') \sum_{m_I} Tr(\rho(m_I, m_I'', m_J'', v, B)) a_{q\pm}^{\{k\}}(m_I, m_I'', m_J'', v, B)}{\sum_v P_v \sum_{m_I'', m_J''} P_{hex}(m_I'', m_J'') \sum_{m_I} Tr(\rho(m_I, m_I'', m_J'', v, B))}, \quad (8)$$

where the sums run over the velocities in the molecular beam v, the nine initial m_I'', m_J'' states and the three m_I states at the surface.

When considering the rotational polarization created with the MMI, the effects of hyperfine depolarization on the initially prepared polarization can be neglected for two reasons; the first of which is that the wavefunction that describes the molecules is propagated through the entire magnetic field profile of the first arm of the apparatus, which includes a zero-field region before the surface. This zero-field region does not result in a complete loss of polarization of the H_2, as the MMI creates initial polarization of both the m_I and m_J states, meaning that unlike the case of polarizations prepared using laser excitation where m_J is polarized and m_I is not, hyperfine depolarization does not lead to a complete loss of polarization of the m_J states. The second reason is the different timescales of the molecule-surface collision, which is typically considered to be orders of magnitude shorter than the μs timescale on which hyperfine depolarization occurs.[34]

III. RESULTS AND DISCUSSION

A. Extrinsic rotational orientation QPDFs created by the magnetic molecular interferometer

As outlined in Sec. II A, the first step to being able to produce the QPDFs of the rotational angular momentum distributions of the ortho-H_2 molecules which collide with the surface is to calculate the $a_{q\pm}^{\{k\}}$ expansion coefficients which quantify the extrinsic polarization as a function of the magnetic field in the solenoid in the first arm of the MMI apparatus. The calculated $a_{q\pm}^{\{k\}}$ moments are presented in Fig. 2 for H_2 molecules with a velocity distribution which is modeled as a Gaussian with a central velocity of 1410 ms^{-1} and a full width at half maximum of 8%, which represents the conditions that are used in a typical specular scattering measurement,[27] and were used in the recent reactivity study for H_2 on Ni(111).[19] The solid black lines in each panel correspond to the incident angle (θ_i) for a specular scattering measurement, which corresponds to

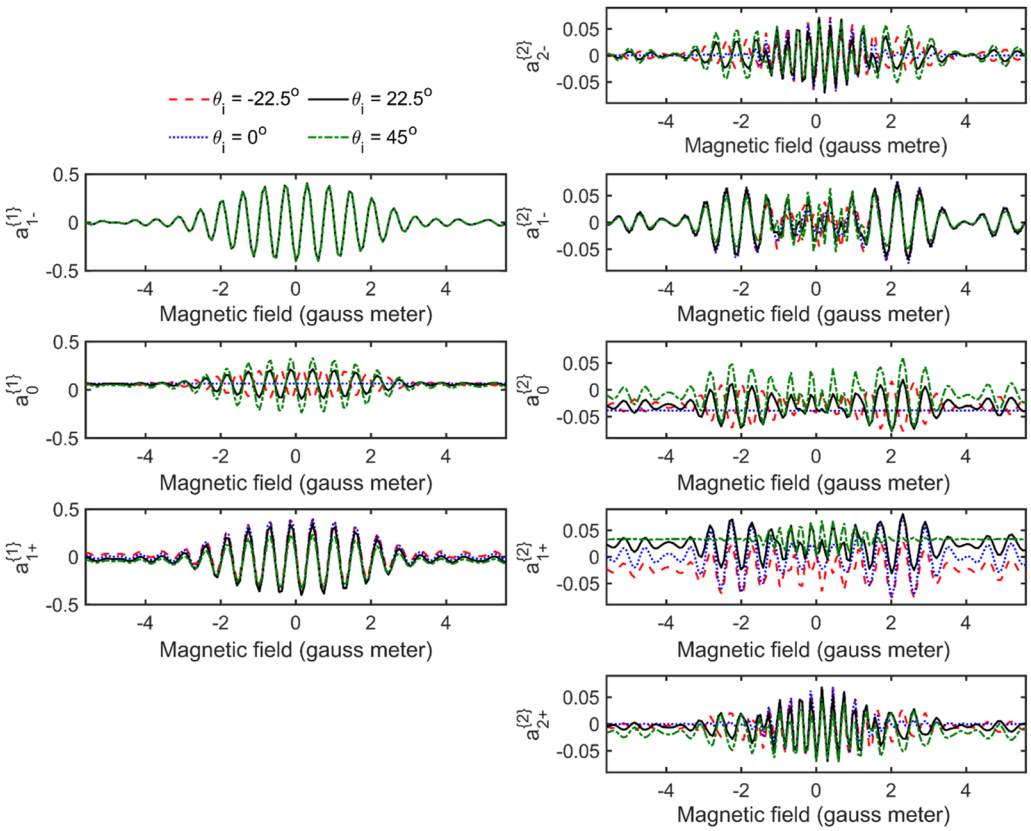

FIG. 2. Calculated real orientation (left column) and alignment (right column) polarization moments of the rotational angular momentum distribution of the H_2 molecules that collide with the surface with a velocity of 1410 ms^{-1} and full width at half maximum of 8% at an incident angle of −22.5° (red dashed line), 0° (blue dotted line), 22.5° (black solid line), and 45° (green dashed-dotted line). The polarization moments have been calculated using the reference frame shown in Fig. 1. A positive θ_i corresponds to ***k*** lying in the −X + Z plane, and a negative value to ***k*** lying in the +X + Z plane.

measurements where the incident and outgoing angle with respect to the surface normal are the same. Focusing on these lines first, the magnitude of the extrinsic polarization moments that the MMI creates is larger for the $k = 1$ moments (shown in the left column of the figure) than the $k = 2$ moments (right column of the figure). Consequently, the MMI will be more sensitive to the intrinsic rotational orientation effects than rotational alignment effects, which govern the molecule–surface interaction. The moments also tend to be larger at lower values of magnetic field, which is due to the velocity spread of the molecular beam used in the calculation of the wavefunction, which leads to dephasing of the polarization of ***J*** at larger values of magnetic fields. If the velocity distribution was narrower, the rate of decay of the oscillations in the polarization moments would be slower and they would continue to oscillate to higher fields. It should also be noted that all the $a_{q\pm}^{\{k\}}$ moments are non-zero as there is no requirement for reflection symmetry or selection rules involved in the preparation of the rotational angular momentum polarization with the MMI, which is not the case when the molecules collide with an achiral surface.[28,31,49]

The different colored lines in each panel show how the polarization that is created changes as a function of θ_i, which is the angle between the incident velocity of the beam and the surface normal (see Fig. 1), and is changed by rotating the surface (see Fig. S1). As the moments change as θ_i changes, the polarization of ***J*** of the molecules that collide with the surface will also change. This is a direct consequence of using the surface normal as the quantization axis, as opposed to the direction of ***k***. The value of $a_{1-}^{\{1\}}$ is independent of θ_i as $a_{1-}^{\{1\}}$ quantifies the orientation with respect to the Y-axis and changing θ_i corresponds to a rotation around that axis. The value of $a_0^{\{1\}}$ decreases as θ_i decreases to the point where it reaches 0 at $\theta_i = 0^\circ$ for all values of the magnetic field, whereas the magnitude of the oscillations in the value of $a_{1+}^{\{1\}}$ increases to a maximum at $\theta_i = 0^\circ$. When $\theta_i = 0^\circ$ the surface normal lies along the direction of the magnetic field that is generated by the solenoid. As a magnetic moment in a magnetic field precesses in the plane perpendicular to the applied field direction, the solenoid changes the polarization within the XY plane but not along the Z-axis when

$\theta_i = 0°$. This means that the moments which quantify the polarization with respect to the Z-axis will not change, which correspond to the $a_0^{\{1\}}$ and $a_0^{\{2\}}$ moments. On the other hand, the change in the polarization along the X-axis is the largest at this incident angle, leading to the largest oscillations in $a_{1+}^{\{1\}}$ at $\theta_i = 0°$. While this is an oversimplification for the case of a hydrogen molecule due to there also being spin-rotation coupling,[56] it provides an intuitive explanation for these trends in the polarization moments. It follows that the sensitivity of the MMI to the different intrinsic polarization moments that define the molecule–surface interaction changes as θ_i is changed.

The precession of the rotational polarization due to the solenoid is shown in the QPDFs presented in Fig. 3 (Multimedia available online), which have been calculated using the polarization moments presented above for $\theta_i = 22.5°$, that is, the specular scattering angle. Figure S2 (Multimedia available online) shows the same precession for $\theta_i = 0°$. The first column of Fig. 3 presents a 3-dimensional "perspective" view with the XZ, YZ and XY projections being shown in the second, third, and fourth columns, respectively. The rotational polarization that the MMI produces at low magnetic fields is strongly oriented in the XY plane, and the main change that changing the magnetic field is to cause a rotation of the polarization in the XY (surface) plane. This can be understood by looking at the polarization moments presented in Fig. 2, as the $a_{1+}^{\{1\}}$ and $a_{1-}^{\{1\}}$ expansion coefficients are largest and change most significantly as a function of the magnetic field, and these quantify the orientation of $\boldsymbol{J}$ with respect to the X and Y axes, respectively.[49] There is some change in polarization with respect to the surface normal (Z-axis), but this is less significant than the changes observed within the surface plane. As changing the rotational polarization

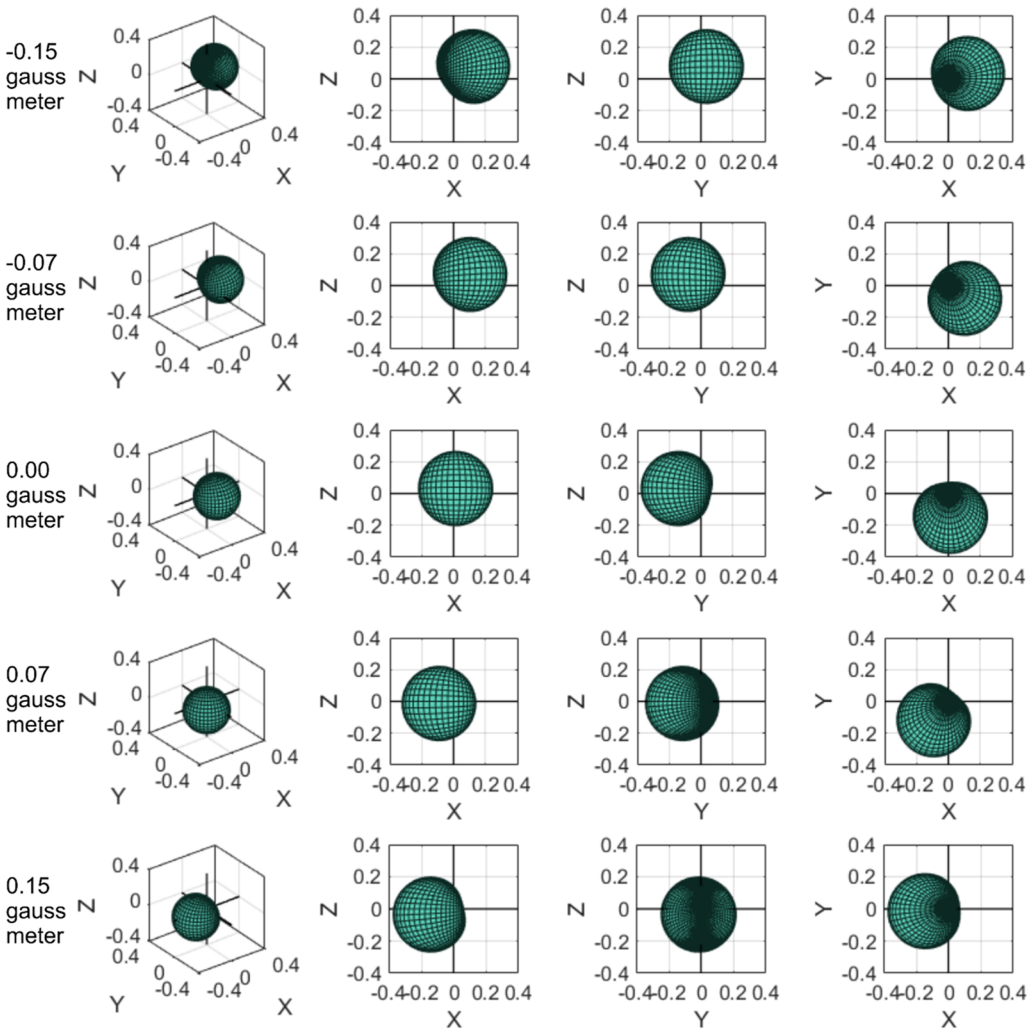

FIG. 3. QPDFs showing the polarization of $\boldsymbol{J}$ as a function of the magnetic field strength in the first solenoid for an incident angle of 22.5°. The left column shows a 3-dimensional "perspective" view, and the second, third and fourth columns 2-dimensional projection plots on to the XZ, YZ, and XY planes, respectively. (Multimedia available online).

with respect to the surface normal could be expected to have a larger effect on reaction or scattering probabilities than changing it within the surface plane, especially for flatter, less corrugated surfaces,[40–43] not being able to significantly change the polarization with respect to the surface normal will reduce the sensitivity of the MMI to these effects which could, in principle, limit what could be measured with the technique.

To help overcome this limitation, a Helmholtz coil has been added to the apparatus at the end of the first arm of the beam line[53] (before the molecules collide with the surface, see Fig. S1) which generates a magnetic field that is perpendicular to the selection axis at the end of the hexapole and the field generated by the solenoid. This field is oriented along the Y-axis and so can rotate the polarization in the XZ (scattering) plane, allowing larger changes in the polarization of $\boldsymbol{J}$ with respect to the Z-axis to be achieved, as is evident from the QPDFs presented in Fig. 4 (Multimedia available online). Therefore, by combining the solenoid field and that generated by the Helmholtz coil, it is also possible to rotate the polarization of $\boldsymbol{J}$ so that it is oriented along the surface normal (Z-axis), increasing the sensitivity of the MMI to polarization effects with respect to this axis.

B. Intrinsic rotational alignment QPDFs created by H_2 surface collisions

In a previous study with the MMI, scattering matrices were obtained for different diffraction peaks for the elastic scattering of H_2 from a Cu(511) surface.[38] The scattering matrices were different for the different diffraction peaks, showing that the underlying dynamics and corresponding vector correlations will also be different. This is shown by the QPDFs in Fig. 5 for a selection of diffraction peaks, and Figs. S3 and S4 which show QPDFs for all the diffraction peaks which were studied. The top row of Fig. 5 (and Fig. S3) shows the average polarization of $\boldsymbol{J}$ that is preferentially scattered into the channel from an initially isotropic rotational angular momentum distribution and so corresponds to the $\boldsymbol{k}$–$\boldsymbol{k}'$–$\boldsymbol{J}$ correlation, whereas the bottom row (and Fig. S4) shows the average polarization of $\boldsymbol{J}'$ that is created when an initially unpolarized beam collides with

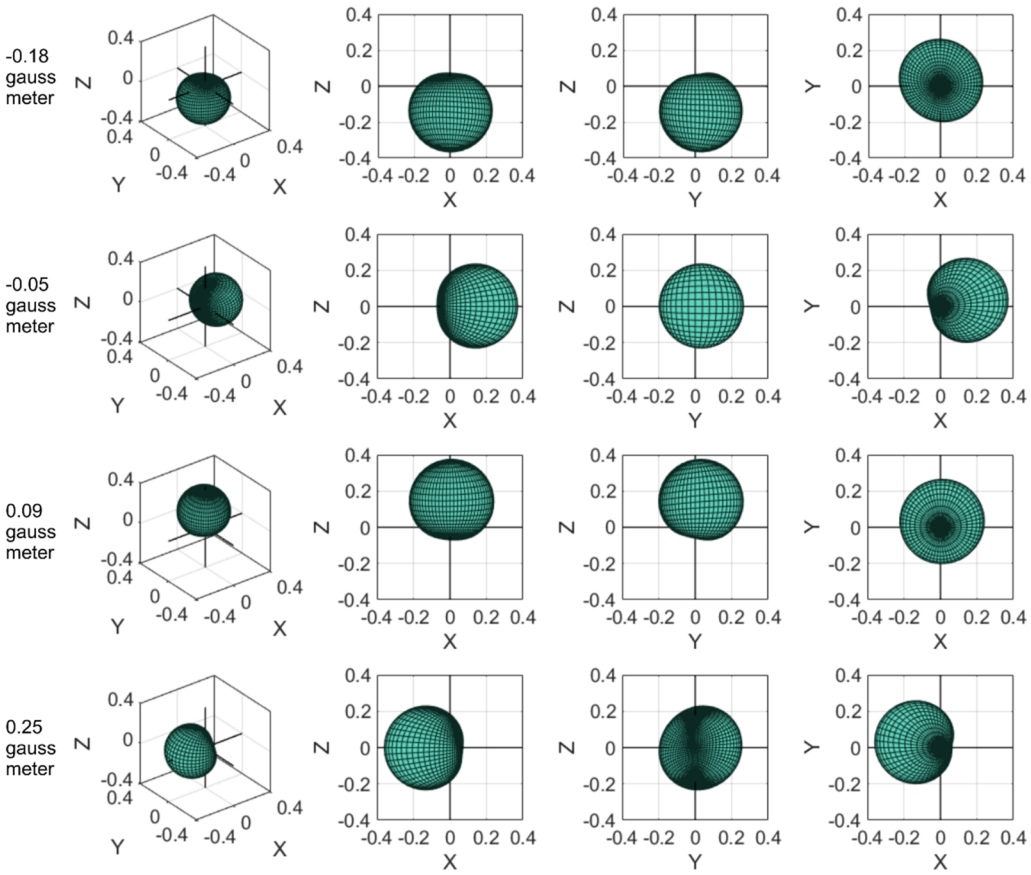

FIG. 4. QPDFs showing the polarization of $\boldsymbol{J}$ which can be obtained by combining both the solenoid and Helmholtz coil[53] for an incident angle of 22.5°, with the field in the solenoid set at −0.15 G m and the Helmholtz field at the values given in the figure. The left column shows a 3-dimensional "perspective" view, and the second, third, and fourth columns two-dimensional projection plots on to the XZ, YZ, and XY planes, respectively. (Multimedia available online).

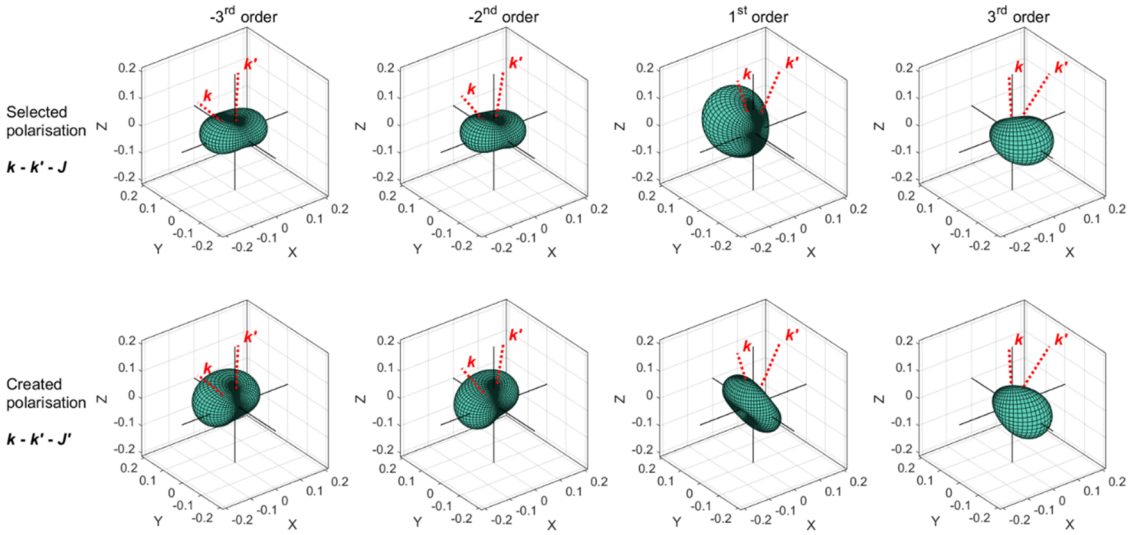

FIG. 5. QPDFs showing the polarization of $\boldsymbol{J}$ for ortho-H_2 molecules that are preferentially scattered into (top row), and scattered from (bottom row) the negative third (first column), negative second (second column), first (third column), and third (fourth column) order diffraction peaks on Cu(511) at an incident energy of 22 meV and a surface temperature of 200 K.[27] The red dashed lines show the direction of $\boldsymbol{k}$ and $\boldsymbol{k}'$ for each diffraction channel, meaning the top row corresponds to the $\boldsymbol{k}$–$\boldsymbol{k}'$–$\boldsymbol{J}$ correlation and the bottom the $\boldsymbol{k}$–$\boldsymbol{k}'$–$\boldsymbol{J}'$ correlation.

the surface, corresponding to the $\boldsymbol{k}$–$\boldsymbol{k}'$–$\boldsymbol{J}'$ correlation. These are presented for a single scattering angle of 45° which is fixed due to the geometry of the MMI apparatus. The non-zero polarization moments are presented in Tables SI and SII of the supplementary material, with the $a_{q\pm}^{\{k\}} \neq 0$ moments corresponding to those which would be expected to be non-zero for achiral scattering,[28,31,49] validating the constraints that have been applied to the S-matrices due to the reflection symmetry.[39]

The first notable feature of the QPDFs is that they are not cylindrically symmetric around the surface normal (Z-axis) and therefore defining the rotational polarization as corresponding to either "helicoptering" or "cartwheeling" with respect to the surface normal (in effect only considering the $a_0^{\{2\}}$ moment) as in previous studies provides a very simplified and somewhat incomplete picture of the underlying rotational polarization. It is also striking that the correlations are similar for some diffraction channels, for example, the negative third order and negative second order, both in terms of the rotational polarization the channel selects and the polarization the channel creates, whereas these are markedly different for the first order (third column) and third order (fourth column) diffraction peaks.

The polarizing properties of the Cu(511) crystal mean that the surface could be used to analyze the rotational polarization of an ortho-H_2 beam, as has been noted previously for the LiF(100) crystal.[26] For example, if a H_2 molecule is "cartwheeling" with $\boldsymbol{J}$ oriented along the +Y-axis, it is more likely to be scattered into the first order diffraction channel, whereas if $\boldsymbol{J}$ is oriented along the −Y-axis it is more likely to be scattered into the third order diffraction channel (compare the QPDFs in the third and fourth panel in the top row of Fig. 5). Comparing the relative intensity of scattering into these two channels could therefore provide information about the polarization of the beam colliding with the surface, allowing the polarization to be analyzed. This also demonstrates that just as the probability that a molecule dissociates on a surface can be controlled by changing the polarization of the incoming molecules,[17–20] scattering intensities into different diffraction channels could also be changed in the same way.[19,26,27]

The Cu(511) surface can also be used as a rotational polarizer as the distributions of $\boldsymbol{J}'$ that scatter into each diffraction channel are different, which was also the case for a LiF(100) crystal.[26] Scattering an isotropic beam of ortho-H_2 from the surface would produce a rotationally polarized beam that is preferentially oriented along the −Y-axis if the molecules that were scattered into the third order diffraction peak were used (bottom row, fourth panel), whereas the polarization created for H_2 scattering into the negative third and negative second order diffraction peaks is more strongly aligned along the X-axis and oriented along the +Y-axis (bottom row, first and second panels).

The QPDFs in the bottom row of Fig. 5 were calculated assuming an unpolarized beam of H_2 collides with the Cu(511) surface. Performing these calculations for an initially rotationally polarized beam of H_2 provides access to the four-vector $\boldsymbol{k}$–$\boldsymbol{k}'$–$\boldsymbol{J}$–$\boldsymbol{J}'$ correlation. The results of this are shown in Fig. 6 for the same diffraction peaks as shown in Fig. 5, and in Figs. S5 and S6 for all diffraction peaks measured in the study presented in Ref. 38, where the initial polarizations of $\boldsymbol{J}$ were chosen to correspond to the initial pure $m_J = 1$ (top row), $m_J = 0$ (middle row) and $m_J = -1$ (bottom row) rotational orientation states shown in the first column. It should be noted that summing over these three m_J resolved QPDFs with the appropriate weights returns the QPDFs in the bottom row of Fig. 5. For scattering into the first order diffraction peak (fourth column)

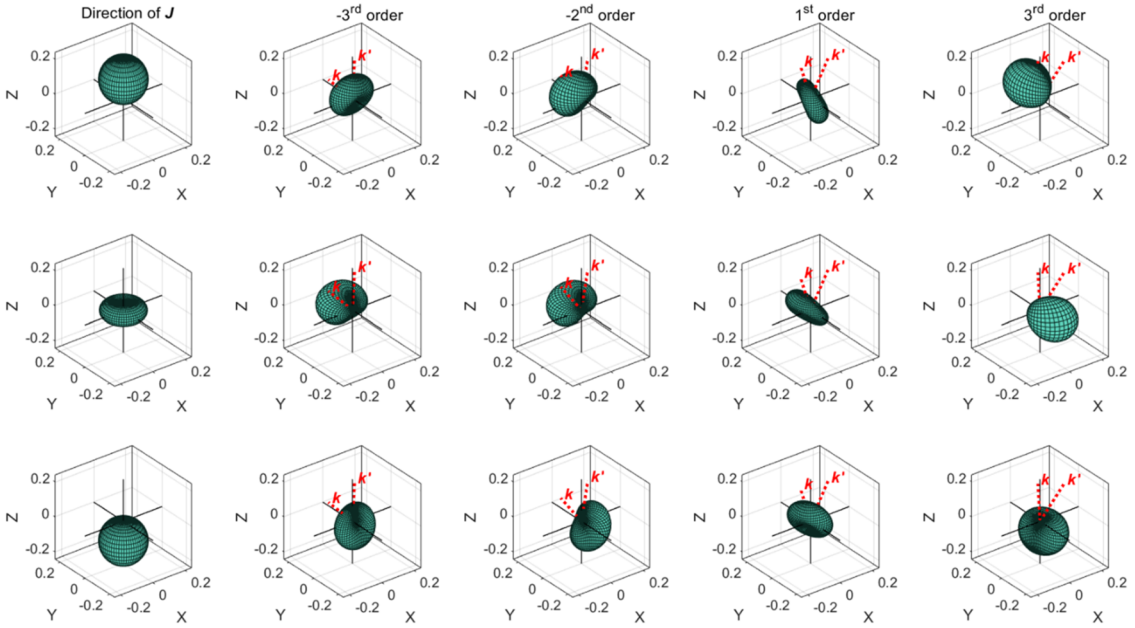

FIG. 6. QPDFs showing the polarization of $\boldsymbol{J'}$ for ortho-H_2 molecules that are scattered from the negative third (second column), negative second (third column), first (fourth column), and third (fifth column) order diffraction peaks on Cu(511) at an incident energy of 22 meV and a surface temperature of 200 K.[27] The initial polarization of $\boldsymbol{J}$ is shown in the first column and corresponds to $m_J = 1$ (top row), $m_J = 0$ (middle row), and $m_J = -1$ (bottom row) states. The red dashed lines show the direction of $\boldsymbol{k}$ and $\boldsymbol{k'}$ for each diffraction channel, meaning these represent the $\boldsymbol{k}$–$\boldsymbol{k'}$–$\boldsymbol{J}$–$\boldsymbol{J'}$ correlation.

the distribution of $\boldsymbol{J'}$ is similar for all three initial m_J states despite them having significantly different initial $\boldsymbol{J}$ polarizations. The distributions of $\boldsymbol{J'}$ are more similar to the initial $\boldsymbol{J}$ distributions for the other diffraction channels, although scattering from $m_J = 0$ tends to result in an oriented scattered beam, despite the initial distribution of $\boldsymbol{J}$ being cylindrically symmetric around the surface normal (Z-axis).

C. Implications for future MMI flux detection measurements

The previous two sections have focused on the H_2 polarization that can be created by the MMI before the molecules hit the surface, which is an extrinsic property that can be controlled, and in the case of the $\boldsymbol{k}$–$\boldsymbol{k'}$–$\boldsymbol{J}$ correlation, the polarization of the molecules that would preferentially be scattered into a channel, which is an intrinsic characteristic of the molecule-surface interaction.[34–37] In previous studies, it has been shown that the general form for a signal (I_{sig}) in terms of extrinsic and intrinsic rotational polarization moments is given by[12,34,36]

$$I_{sig} \propto \sum_{k=0}^{2J} \sum_{q=-k}^{k} \frac{2k+1}{2} a_q^{(k)} A_q^{(k)*}, \tag{9}$$

where $a_q^{(k)}$ is the intrinsic moment and $A_q^{(k)}$ the extrinsic moment. The signal that is measured from an experiment depends on both of these properties; for example, if a measurement is done where no stereodynamic effects are observed this could be attributed to the initial beam being unpolarized [$A_q^{(k)} = 0$ unless $k = q = 0$], the scattering process being independent of the rotational polarization of the molecule [$a_q^{(k)} = 0$ unless $k = q = 0$], or both.

In the case of the MMI, measurements that are sensitive to the $\boldsymbol{k}$–$\boldsymbol{k'}$–$\boldsymbol{J}$ correlation are referred to as flux detection measurements.[19,33] These correspond to those where the magnetic field in the first arm is scanned to change the rotational orientation of the molecules that collide with the surface, and the molecules that are scattered into the channel of interest are detected regardless of their final state. In terms of the scattering matrix, the expression for the flux detection signal (I_{FD}) can be written as

$$I_{FD} \propto \sum_{v} P_v \sum_{m_I'', m_J''} P_{Hex}(m_I'', m_J'') \sum_{m_I} \left\langle \psi \middle| S^{\dagger} S \middle| \psi \right\rangle. \tag{10}$$

It can be shown that the flux detection signal can also be written in an analogous way to that developed previously for gas-phase studies[12,34,36] using the idea of intrinsic and extrinsic polarization moments. In terms of the real polarization moments, the signal can be written as

$$I_{FD} \propto \sum_{k=0}^{2J} \frac{2k+1}{2} \left[A_0^{\{k\}} a_0^{\{k\}} + \sum_{q=1}^{k} A_{q+}^{\{k\}} a_{q+}^{\{k\}} - A_{q-}^{\{k\}} a_{q-}^{\{k\}} \right], \tag{11}$$

where the $A_{q\pm}^{\{k\}}$ moments correspond to those calculated from the wavefunction using the methods outlined in Sec. II C, and the $a_{q\pm}^{\{k\}}$ moments to those that describe the $\boldsymbol{k}$–$\boldsymbol{k'}$–$\boldsymbol{J}$ correlation and that have been calculated from the S-matrix as described in Sec. II B.

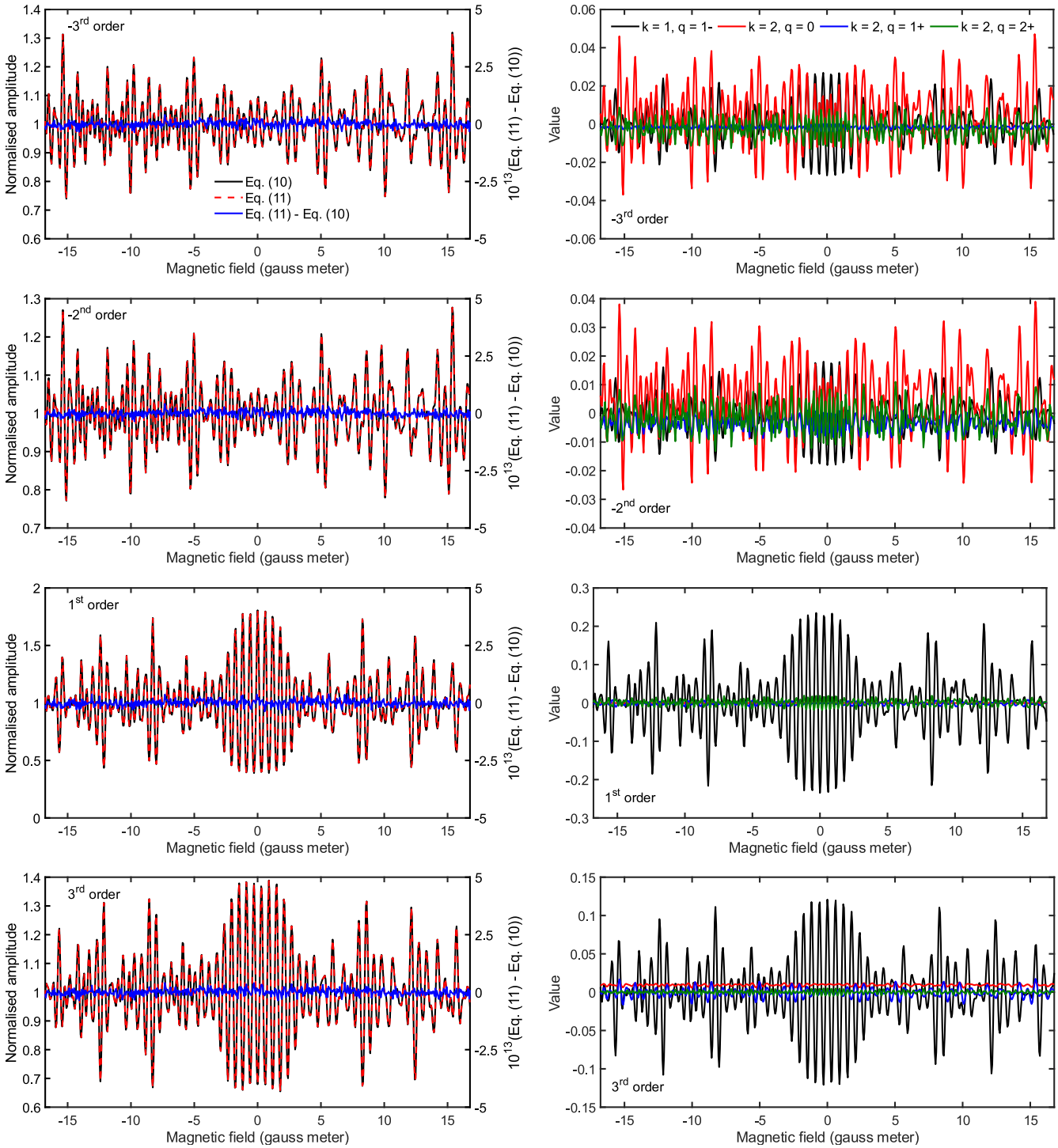

FIG. 7. Comparison of flux detection signals (left column) calculated using Eq. (10) (black solid line) and Eq. (11) (red dashed line), and the (magnified) difference between them (blue solid line) and the contribution the $a_{1-}^{\{1\}}$ (black), $a_{0}^{\{2\}}$ (red), $a_{1+}^{\{2\}}$ (blue), and $a_{2+}^{\{2\}}$ (green) polarization moments make to the signal (right column) for H_2 scattering into the negative third order (top row), negative second order (second row), first order (third row), and third order (bottom row) diffraction peaks in a collision with Cu(511) at a surface temperature of 200 K at an incident energy of 22 meV.

The explicit expression for the flux detection signal in terms of the scattering matrix elements is given in Eq. (S4).

The equivalence of Eqs. (10) and (11) is demonstrated in the left column of Fig. 7, which presents flux detection signals calculated using Eq. (10) (black line) and Eq. (11) (dashed red line), and the difference between them (blue line), for H_2 scattering from Cu(511) for the different diffraction peaks that are considered in Figs. 5 and 6. As can be seen, the signals calculated are indistinguishable (note the greatly magnified scale of the difference between the signals on the right-hand axis). The oscillations in the data persist to higher values of magnetic field than in Fig. 2 as the velocity distribution that contributes to signals from diffraction channels is narrower than those for specular scattering. The contribution each of the $a_{q\pm}^{\{k\}}$ moments makes to the flux detection signals are shown in the right column of the figure, with the contribution of the $a_0^{\{2\}}$ moment being largest for the two negative diffraction peaks and $a_{1-}^{\{1\}}$ moment for the two positive diffraction peaks. It is however interesting to note that the values of the $a_{1-}^{\{1\}}$ and $a_0^{\{2\}}$ moments are similar for the third order diffraction peak, as shown in Table SI, but the greater sensitivity of the MMI to the $a_{1-}^{\{1\}}$ moment compared to the $a_0^{\{2\}}$ moment (see Fig. 2) means that this dominates the signal.

This means that in the future, there are two different methods that can be used to analyze flux detection measurements, using Eq. (10) which will give $S^\dagger S$, or using Eq. (11) which produces a set of polarization parameters. While there is unquestionably value in both, it is more difficult to gain physical insight about the collision from the $S^\dagger S$ matrix; the diagonal elements quantify the relative probabilities of the H_2 molecules that are initially in $m_J = 1$, $m_J = 0$ and $m_J = -1$ with respect to the surface normal scattering into the channel, but the amplitudes and phases of the off-diagonal elements do not provide any immediate and intuitive insight into the dynamics of the collision [see Eqs. (S5) and (S6)]. On the other hand, the intrinsic polarization moments that are obtained using Eq. (11) have physically significant meanings, in the sense that they quantify the rotational polarization dependence of the collision with respect to various axes, as given in Table I of Ref. 49. They also allow stereodynamical portraits to be produced, which provides a picture of the rotational polarization of the molecules that preferentially scatter into the channel under investigation. This capability therefore provides a more immediate insight into the stereodynamic effects underpinning the collision than the extraction of $S^\dagger S$ from the measurements. It also provides a more complete picture than just considering the rotational polarization moments along the Z-axis, which in effect only considers the effect of the polarization moments where $q = 0$.

IV. SUMMARY

The current work has presented quantum population distribution functions, or "stereodynamical portraits,"[12,34,35,37,44–46] to visualize the polarization of the rotational angular momentum of ortho-H_2 molecules that can be created by the magnetic molecular interferometer[26,27,33,38,51] before they collide with a surface. The strongest polarization corresponds to orientation of $\boldsymbol{J}$ in the XY (surface) plane, which then precesses in that plane as the solenoid current is changed. A second perpendicular magnetic field, generated using a Helmholtz coil, can be used to rotate the polarization of $\boldsymbol{J}$ out of the XY plane so that it can be oriented along the surface normal (Z-axis). The combination of these two fields therefore allows $\boldsymbol{J}$ to be oriented along either the X-, Y-, or Z-axis in future stereodynamic experiments, increasing the sensitivity of the MMI to the three-dimensional rotational orientation dependence of the molecule–surface interaction.

The same methodology has also been used in conjunction with scattering matrices determined from a previous study to depict the polarization of the H_2 molecules that can be selected and created when an initially unpolarized beam is scattered into different diffraction channels from the Cu(511) surface.[38] The rotational polarization of the H_2 molecules that are preferentially scattered into each of the channels, and scattered from the channels, can be markedly different for each of the diffraction channels, allowing the surface to be used both to analyze the polarization of an incident H_2 molecular beam with unknown polarization, and to create a polarized beam if an initially unpolarized beam is scattered from the surface. These QPDFs can also be produced for the case of initially rotationally polarized beams of H_2 molecules, which provides access to the full $\boldsymbol{k}$–$\boldsymbol{k}'$–$\boldsymbol{J}$–$\boldsymbol{J}'$ correlation. The distribution of $\boldsymbol{J}'$ of the scattered molecules depends on the rotational polarization of the H_2 molecules that collide with the surface and again varies for each of the diffraction peaks.

Furthermore, the work has highlighted a new method for analyzing signals obtained from flux detection experiments performed with the MMI, which provide a measure of the $\boldsymbol{k}$–$\boldsymbol{k}'$–$\boldsymbol{J}$ correlation. Using this, it would, at least in principle, be possible to extract the $a_{q\pm}^{\{k\}}$ polarization moments from the data that characterize this correlation, which can then be used to provide a more physical picture of the stereodynamics than is possible through the extraction of the $S^\dagger S$ matrix. While it would not be possible to use the same method for the analysis of full interferometer measurements[26,27,33,38] from the MMI, it is possible to extract an S-matrix from data measured in this way, which as demonstrated allows the visualization of the $\boldsymbol{k}$–$\boldsymbol{k}'$–$\boldsymbol{J}$–$\boldsymbol{J}'$ correlation.

SUPPLEMENTARY MATERIAL

The supplementary material comprises videos showing the precession of $\boldsymbol{J}$ in the magnetic fields generated by the solenoid and Helmholtz coils at an incident angle of 22.5°, as well as a figure and a video showing the precession caused by the solenoid field at an incident angle of 0°. A schematic of the MMI apparatus is also presented showing the direction of the magnetic fields and quantization axes that define the reference frames used in the calculations. Additional figures showing the QPDFs for all the diffraction peaks for H_2 scattering from Cu(511) are given for the $\boldsymbol{k}$–$\boldsymbol{k}'$–$\boldsymbol{J}$, $\boldsymbol{k}$–$\boldsymbol{k}'$–$\boldsymbol{J}'$ and $\boldsymbol{k}$–$\boldsymbol{k}'$–$\boldsymbol{J}$–$\boldsymbol{J}'$ correlations alongside the values of the $a_{q\pm}^{\{k\}}$ moments for the three vector correlations. The explicit expression for the flux detection signal measured using the MMI is also given in terms of the scattering matrix elements.

ACKNOWLEDGMENTS

The author thanks Gil Alexandrowicz for helpful discussions, guidance, and reading a draft of the manuscript, and Chris Baker

for supplying the magnetic field profile for the Helmholtz coils. The project was funded by a UKRI Future Leaders Fellowship (Grant No. MR/X03609X/1) and an EPSRC standard (Grant No. EP/X037886/1).

AUTHOR DECLARATIONS

Conflict of Interest

The author has no conflicts to disclose.

Author Contributions

Helen Chadwick: Conceptualization (lead); Data curation (lead); Formal analysis (lead); Funding acquisition (lead); Investigation (lead); Methodology (lead); Writing – original draft (lead); Writing – review & editing (lead).

DATA AVAILABILITY

The data that support the findings of this study are available from the corresponding author upon reasonable request.

REFERENCES

[1]M. L. Costen, S. Marinakis, and K. G. McKendrick, Chem. Soc. Rev. **37**, 732 (2008).
[2]T. R. Sharples, J. G. Leng, T. F. M. Luxford, K. G. McKendrick, P. G. Jambrina, F. J. Aoiz, D. W. Chandler, and M. L. Costen, Nat. Chem. **10**, 1148 (2018).
[3]A. S. Mullin, Annu. Rev. Phys. Chem. **76**, 357 (2025).
[4]H. Chadwick, M. Brouard, T. Perkins, and F. J. Aoiz, Int. Rev. Phys. Chem. **33**, 79 (2014).
[5]K. T. Lorenz, D. W. Chandler, J. W. Barr, W. Chen, G. L. Barnes, and J. I. Cline, Science **293**, 2063 (2001).
[6]C. G. Heid, V. Walpole, M. Brouard, P. G. Jambrina, and F. J. Aoiz, Nat. Chem. **11**, 662 (2019).
[7]C. G. Heid, I. P. Bentham, V. Walpole, P. G. Jambrina, F. J. Aoiz, and M. Brouard, J. Phys. Chem. Lett. **12**, 310 (2021).
[8]H. Chadwick, B. Nichols, S. D. S. Gordon, B. Hornung, E. Squires, M. Brouard, J. Kłos, M. H. Alexander, F. J. Aoiz, and S. Stolte, J. Phys. Chem. Lett. **5**, 3296 (2014).
[9]M. McCrea, M. Strutton, J. Featherstone, C. G. Heid, M. Brouard, P. G. Jambrina, and F. J. Aoiz, J. Chem. Phys. **162**, 154306 (2025).
[10]M. Brouard, D. H. Parker, and S. Y. T. van de Meerakker, Chem. Soc. Rev. **43**, 7279 (2014).
[11]G. Tang, M. Besemer, J. Onvlee, T. Karman, A. van der Avoird, G. C. Groenenboom, and S. Y. T. van de Meerakker, J. Chem. Phys. **156**, 214304 (2022).
[12]M. Brouard and C. Vallance, *Tutorials in Molecular Reaction Dynamics* (Royal Society of Chemistry, Cambridge, 2010).
[13]A. J. Orr-Ewing and R. N. Zare, Annu. Rev. Phys. Chem. **45**, 315 (1994).
[14]Y. Wang, J. Huang, W. Wang, T. Du, Y. Xie, Y. Ma, C. Xiao, Z. Zhang, D. H. Zhang, and X. Yang, Science **379**, 191 (2023).
[15]W. E. Perreault, N. Mukherjee, and R. N. Zare, Science **358**, 356 (2017).
[16]U. Heinzmann, S. Holloway, A. W. Kleyn, R. E. Palmer, and K. J. Snowdon, J. Phys.: Condens. Matter **8**, 3245 (1996).
[17]B. L. Yoder, R. Bisson, and R. D. Beck, Science **329**, 553 (2010).
[18]H. Ueta and M. Kurahashi, Angew. Chem., Int. Ed. **56**, 4174 (2017).
[19]H. Chadwick, G. Zhang, C. J. Baker, P. L. Smith, and G. Alexandrowicz, Nat. Commun. **16**, 4625 (2025).
[20]H. Hou, S. J. Gulding, C. T. Rettner, A. M. Wodtke, and D. J. Auerbach, Science **277**, 80 (1997).
[21]G. O. Sitz, A. C. Kummel, and R. N. Zare, J. Chem. Phys. **89**, 2558 (1988).
[22]G. O. Sitz, A. C. Kummel, R. N. Zare, and J. C. Tully, J. Chem. Phys. **89**, 2572 (1988).
[23]A. C. Luntz, A. W. Kleyn, and D. J. Auerbach, Phys. Rev. B **25**, 4273 (1982).
[24]P. Floß, C. S. Reilly, D. J. Auerbach, and R. D. Beck, Front. Chem. **11**, 1238711 (2023).
[25]C. S. Reilly, D. J. Auerbach, L. Zhang, H. Guo, and R. D. Beck, Science **387**, 962 (2025).
[26]Y. Alkoby, H. Chadwick, O. Godsi, H. Labiad, M. Bergin, J. T. Cantin, I. Litvin, T. Maniv, and G. Alexandrowicz, Nat. Commun. **11**, 3110 (2020).
[27]H. Chadwick and G. Alexandrowicz, Faraday Discuss. **251**, 76 (2024).
[28]B. G. Perkins, Jr. and D. J. Nesbitt, J. Phys. Chem. A **114**, 1398 (2010).
[29]D. J. Auerbach, J. C. Tully, and A. M. Wodtke, Nat. Sci. **1**, e10005 (2021).
[30]M. P. de Miranda and D. C. Clary, J. Chem. Phys. **106**, 4509 (1997).
[31]F. J. Aoiz, M. Brouard, and P. A. Enriquez, J. Chem. Phys. **105**, 4964 (1996).
[32]J. D. Barnwell, J. G. Loeser, and D. R. Herschbach, J. Phys. Chem. **87**, 2781 (1983).
[33]O. Godsi, G. Corem, Y. Alkoby, J. T. Cantin, R. V. Krems, M. F. Somers, J. Meyer, G. J. Kroes, T. Maniv, and G. Alexandrowicz, Nat. Commun. **8**, 15357 (2017).
[34]J. Aldegunde, M. P. de Miranda, J. M. Haigh, B. K. Kendrick, V. Sáez-Rábanos, and F. J. Aoiz, J. Phys. Chem. A **109**, 6200 (2005).
[35]J. Aldegunde, F. J. Aoiz, V. Sáez-Rábanos, B. K. Kendrick, and M. P. de Miranda, Phys. Chem. Chem. Phys. **9**, 5794 (2007).
[36]J. Aldegunde, F. Javier Aoiz, and M. P. de Miranda, Phys. Chem. Chem. Phys. **10**, 1139 (2008).
[37]J. Aldegunde, J. M. Alvariño, B. K. Kendrick, V. Sáez Rábanos, M. P. de Miranda, and F. J. Aoiz, Phys. Chem. Chem. Phys. **8**, 4881 (2006).
[38]H. Chadwick and G. Alexandrowicz, J. Phys. Chem. C **128**, 20913 (2024).
[39]H. Chadwick, M. F. Somers, A. C. Stewart, Y. Alkoby, T. J. D. Carter, D. Butkovicova, and G. Alexandrowicz, Nat. Commun. **13**, 2287 (2022).
[40]L. Y. Wu, M. J. Roman, B. R. Heazlewood, and M. Kurahashi, Phys. Chem. Chem. Phys. **27**, 5701 (2025).
[41]M. J. E. de Willigen, M. Kurahashi, and L. B. F. Juurlink, Phys. Chem. Chem. Phys. **24**, 18227 (2022).
[42]Y. Tsuda, J. S. Gueriba, H. Ueta, W. A. Diño, M. Kurahashi, and M. Okada, JACS Au **2**, 1839 (2022).
[43]M. Kurahashi, J. Chem. Phys. **151**, 084702 (2019).
[44]M. P. de Miranda and F. J. Aoiz, Phys. Rev. Lett. **93**, 083201 (2004).
[45]M. P. de Miranda, F. J. Aoiz, V. Sáez-Rábanos, and M. Brouard, J. Chem. Phys. **121**, 9830 (2004).
[46]M. Brouard, H. Chadwick, C. J. Eyles, F. J. Aoiz, and J. Kłos, J. Chem. Phys. **135**, 084305 (2011).
[47]R. C. Mowrey and G. J. Kroes, J. Chem. Phys. **103**, 1216 (1995).
[48]I. V. Hertel and W. Stoll, Adv. At. Mol. Phys. **13**, 113 (1978).
[49]M. P. de Miranda, F. J. Aoiz, L. Bañares, and V. S. Rábanos, J. Chem. Phys. **111**, 5368 (1999).
[50]H. Chadwick, Phys. Chem. Chem. Phys. **26**, 19630 (2024).
[51]H. Chadwick, Y. Alkoby, J. T. Cantin, D. Lindebaum, O. Godsi, T. Maniv, and G. Alexandrowicz, Phys. Chem. Chem. Phys. **23**, 7673 (2021).
[52]A. P. Jardine, P. Fouquet, J. Ellis, and W. Allison, Rev. Sci. Instrum. **72**, 3834 (2001).
[53]I. Litvin, Y. Alkoby, O. Godsi, G. Alexandrowicz, and T. Maniv, Results Phys. **12**, 381 (2019).
[54]C. Krüger, E. Lisitsin-Baranovsky, O. Ofer, P. A. Turgeon, J. Vermette, P. Ayotte, and G. Alexandrowicz, J. Chem. Phys. **149**, 164201 (2018).
[55]Y. Alkoby, "Studying molecule-surface interactions using magnetically manipulated molecular beams," Ph.D. thesis, Swansea University, 2022.
[56]N. F. Ramsey, Phys. Rev. **85**, 60 (1952).